Corrosion Science 87 (2014) 187–198

Contents lists available at ScienceDirect

Corrosion Science

journal homepage: www.elsevier.com/locate/corsci

Design and synthesis of a novel class of inhibitors for mild steel corrosion in acidic and carbon dioxide-saturated saline media

Mohammad A.J. Mazumder [a], Hasan A. Al-Muallem [a], Mohamed Faiz [b], Shaikh A. Ali [a,*]

[a] Chemistry Department, King Fahd University of Petroleum and Minerals, Dhahran 31261, Saudi Arabia
[b] Physics Department, King Fahd University of Petroleum and Minerals, Dhahran 31261, Saudi Arabia

ARTICLE INFO

Article history:
Received 7 January 2014
Accepted 7 June 2014
Available online 18 June 2014

Keywords:
A. Mild steel
B. Polarization
B. Weight loss
C. Acid corrosion
C. Interfaces
C. Thermodynamic diagrams

ABSTRACT

p-(9-(2-Methylisoxazolidin-5-yl)nonyloxy)benzaldehyde **I**, prepared using a cycloaddition protocol, was elaborated into its cinnamaldehyde derivative **II** which upon quarternization with propargyl chloride afforded **III** bearing an interesting blend of structural traits suitable for imparting inhibition of mild steel corrosion. Novel compounds **I–III** showed efficient inhibition against mild steel corrosion in CO_2–0.5 M NaCl (40 °C, 1 atm; 120 °C, 10 bar), 1, 4, 7.7 M HCl, and 0.5 M H_2SO_4 at 60 °C as determined by gravimetry and electrochemical methods. The presence of carbonaceous surface and nitrogen, as revealed by XPS study, indicated the formation of a film covering the metal surface, which imparted corrosion inhibition.

1. Introduction

A molecular framework as depicted in Fig. 1, has structural motifs of propargyl, cinnamaldehyde, isoxazolidine as well as a hydrophobe, all known for their excellent efficacies in arresting mild steel corrosion (*vide infra*). It would indeed be an intriguing experience to embed such a multitude of structural traits in a single molecule, which could then be studied for inhibition efficacy with great anticipation. To alleviate the enormous economic losses incurred because of corrosion, there would always be room for better designing of novel inhibitor molecules that could withstand the rigor of corrosive environments in protecting metal such as mild steel. A significant portion (≈30%) of the economic losses in the oil and gas industry is due to failures of mild steel pipelines, which encounter several corrosive environments [1–3]. Crude oil itself is corrosive; carbon dioxide, present in gas or injected into oil wells to increase its production [4], is also corrosive. Mild steel also undergoes severe corrosive attack during industrial acid cleaning.

The corrosive attack in the HCl medium is explained using the following reactions 1–5 in anode and 6–8 in cathode [5,6]:

Anodic dissolution of Fe:

$$Fe + Cl^- \leftrightharpoons (FeCl^-)_{ads} \quad (1)$$

$$(FeCl^-)_{ads} \leftrightharpoons (FeCl)_{ads} + e^- \quad (2)$$

$$(FeCl)_{ads} \rightarrow FeCl^+ + e^- \quad (3)$$

$$FeCl^+ \leftrightharpoons Fe^{2+} + Cl^- \quad (4)$$

$$(FeCl^-)_{ads} + Inh^+ \leftrightharpoons (FeCl^- \cdots Inh^+)_{ads} \quad (5)$$

Cathodic evolution of H_2:

$$Fe + H^+ \leftrightharpoons (FeH^+)_{ads} \quad (6)$$

$$(FeH^+)_{ads} + e^- \rightarrow (FeH)_{ads} \quad (7)$$

$$(FeH)_{ads} + H^+ + e^- \rightarrow Fe + H_2 \quad (8)$$

$$Fe + Inh^+ \leftrightharpoons (FeInh^+)_{ads} \quad (9)$$

The detrimental reactions are retarded by consecutive adsorption of a chloride ion and a cationic inhibitor (Inh^+) as described in step (5) which restricts the steps (2)–(4) from happening. The corrosion by cathodic evolution of hydrogen, on the other hand, can be minimized by effective competition of the Inh^+ with H^+ (step 6 vs. step 9).

The nature of anions is known to influence the efficiency of corrosion inhibition by ammonium salts [7]; while they are excellent inhibitors in HCl but poor inhibitors in H_2SO_4 [8]. The positive surface charge of iron in both the acidic media, because of the

* Corresponding author. Tel.: +966 13 860 3830; fax: +966 13 860 4277.
E-mail address: shaikh@kfupm.edu.sa (S.A. Ali).
URL: http://faculty.kfupm.edu.sa/CHEM/shaikh/ (S.A. Ali).

http://dx.doi.org/10.1016/j.corsci.2014.06.026
0010-938X/

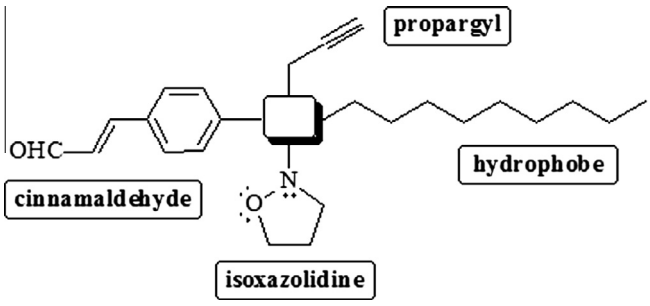

Fig. 1. Design of corrosion inhibitor bearing several structural motifs in a single molecular framework.

corrosion potential E_{corr} being more positive than the potential for zero charge (PZC) $E_{q=0}$, discourages the adsorption of organic cations [9]. However, the stronger adsorbability of the Cl^- in compare to SO_4^{2-} [10,11], shifts the PZC ($E_{q=0}$) towards more positive values than the E_{corr}, thereby allowing the electrostatic adsorption of inhibitor ions Inh^+ [12]. The film of $(FeCl^-\cdots Inh^+)_{ads}$ imparts protection against corrosive HCl media. Note that the inhibitive efficiencies of organic cationic inhibitors in H_2SO_4 media increases significantly in the presence of halide ions [13]. Since the first introduction of isoxazolidines to the corrosion literature [14], our continued efforts have established that these compounds bearing long chain hydrophobic substituents are effective inhibitors both in H_2SO_4 and HCl media [15–17]. Diallylamines bearing long chain hydrophobe and alkyne substituents also imparted very good protection in both the acidic media [18]. The mechanisms through which the corrosion inhibitors function have been ascribed to adsorption processes on either or both the anode or cathode. The formation of a good protective film (coating) on the metal surface essentially requires an inhibitor molecule to have a (1) hydrophilic polar end (e.g. cationic group), (2) a long alkyl chain to form a hydrophobic barrier, and (3) functional group like alkyne or a cinnamyl moiety which can undergo H atom-initiated polymerization between the adsorbed inhibitor molecules [19–21]. Many inhibitors undergo physisorption on the metal surface [22], while inhibitors having nonbonded- and π-electrons may undergo chemisorption [23].

The CO_2 corrosion is explained using the reactions described in steps (10)–(16). It is the carbonic acid (not the dry CO_2) which, at the same pH, has been found to be more aggressive than hydrochloric acid [24] for attacks to mild steel pipelines [25] as a result of the reaction steps (12)–(16) [26]:

$$CO_2(g) \rightleftharpoons CO_2(aq) \tag{10}$$

$$CO_2(aq) + H_2O \rightleftharpoons H_2CO_3(aq) \rightleftharpoons HCO_3^-(aq) + H^+(aq) \tag{11}$$

$$Fe(s) + 2H_2CO_3(aq) \rightleftharpoons Fe(HCO_3)_2(aq) + H_2(g) \tag{12}$$

$$Fe(s) + 2H^+(aq) \rightleftharpoons Fe^{2+}(aq) + H_2(g) \tag{13}$$

$$Fe^{2+}(aq) + 2H_2O \rightleftharpoons Fe(OH)_2(s) + 2H^+(aq) \tag{14}$$

$$Fe(OH)_2(s) \rightleftharpoons FeO(s) + H_2O \tag{15}$$

$$Fe(HCO_3)_2(aq) \rightleftharpoons FeCO_3(s) + H_2CO_3(aq) \tag{16}$$

Corrosion inhibitors bearing hetero-atoms of N, O, P, or S having non-bonded electrons and long chain hydrophobes are used when the formation of a protective ($FeCO_3$) layer [27,28], which helps reduce the corrosive attack, is not favorable [29–31]. $FeCO_3$ is less soluble at high temperatures and pH values; as such higher temperatures usually decrease the corrosion rate because of formation of the more stable surface films [32–34]. Electron-rich imidazolines are extensively used to minimize corrosion in the oil and gas industry [30,35–40].

Inadequate unraveling of the complex mechanism of CO_2 corrosion has become the impediment in designing new inhibitors [41,42]. The effective commercial formulations used in the corrosion inhibition of oil field steel are mixtures of surface-active compounds: *N*-containing compounds, acetylenic compounds, surfactants, and aldehydes. It is our objective to put together cationic charges, hydrophobic environment, alkyne, and cinnamyl motifs in a novel class of inhibitor molecules (Fig. 2) and evaluate their effectiveness in arresting corrosion attack on mild steel in various corrosive media.

2. Experimental

2.1. Materials

Paraformaldehyde, 10-undecenyl bromide, propargyl chloride, p-hydroxybenzaldehyde, and *N*-methylhydroxyamine hydrochloride, malonic acid, manganese dioxide, piperidine, silica gel 100, obtained from Fluka Chemie AG, were used as received. Sodium chloride of >99.5 purity from Baker Chemical Company was used for the inhibition study.

2.2. Physical methods

The chemical composition of the inhibitor compounds were measured by ^{1}H NMR spectra (500 MHz, JEOL, Japan) in $CDCl_3$, and tetramethylsilane was used as an internal reference. All chemical shifts were reported in parts per million (ppm). The structural composition of all inhibitor molecules were determined by Fourier Transform Infrared (FT-IR) spectrometer (Nicolet Avatar-380). Potentiostat (Model 283, EG&G PARC) was used for the electrochemical measurements. R&D Autoclave Bolted Closure System (Model # 401C-0679 from Autoclave Engineers), Control System interfaced with Computer, and PC with monitor (High Tech Engineering, India) has been installed for the study of corrosion inhibition under higher temperature and pressure.

2.3. Synthesis

2.3.1. Synthesis of p-undec-10-enyloxybenzaldehyde (3)

The following reaction was carried out in the presence of N_2. To a stirring solution of sodium ethoxide (0.065 mol; prepared by adding 1.5 g sodium in 30 cm^3 ethanol) was added *p*-hydroxybenzaldehyde **(1)** (7.95 g, 0.065 mmol) at 20 °C. After the mixture became homogeneous (*ca.* 5 min), 11-bromo-1-undecene **(2)** (15.2 g, 0.065 mol) was added and the mixture was heated at 65 °C for 12 h and at 90 °C for a further period of 12 h. The concentrated residue in ether (50 cm^3) was washed with water (2 × 100 cm^3), 5% NaOH solution (2 × 50 cm^3), followed again by water (2 × 50 cm^3). The organic layer was dried and concentrated to give *p*-undec-10-enyloxybenzaldehyde **(3)** (18.7 g, 88.7%) as a brown liquid. ^{1}H NMR spectrum revealed the product as very pure, and as such used without further purification.

2.3.2. Reaction N-methyl nitrone 4 with alkene 3: Synthesis of adduct p-(9-(2-methylisoxazolidin-5-yl)nonyloxy)benzaldehyde (5)

To a mixture of *N*-methylhydroxylamine hydrochloride (5.00 g, 60 mmol) in ethanol (45 cm^3) was added sodium acetate-trihydrate (8.84 g, 65 mmol) followed by paraformaldehyde (2.7 g, 90 mmol). After stirring under N_2 at 65 °C for 40 min to generate nitrone **4**, alkene **3** (17.3 g, 63 mmol) was added, and the reaction mixture in a pressure-vessel was then heated at 100 °C for 8 h.

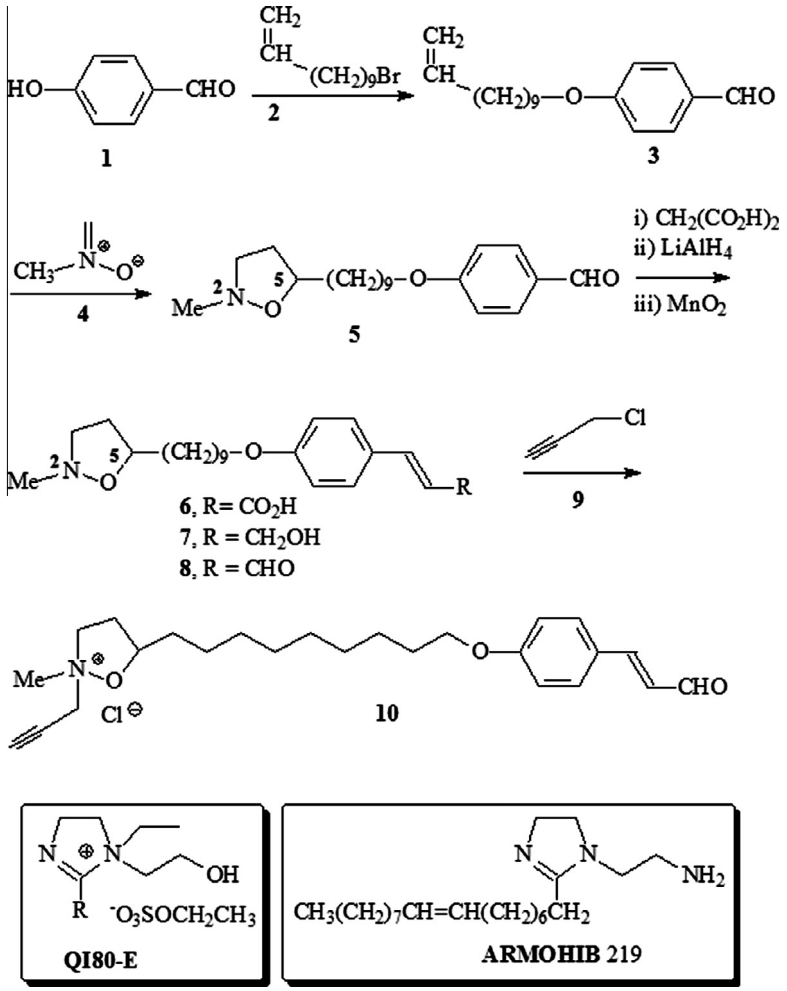

Fig. 2. Synthesis of inhibitor molecules.

Ethanol was removed and water (50 cm^3) was added to the residue, and solid $NaHCO_3$ was added to neutralize the solution. The aqueous layer was extracted with ether (3×75 cm^3). The ether solution was dried, concentrated, and the crude product upon chromatographic purification using ether as the eluent gave adduct **5** (white solid, 18.9 g, 90%). Mp 52–53 °C (ether-hexane).

*2.3.3. p-(9-(1-Methylisoxazolidin-5-yl)nonyloxy)cinnamic acid (**6**)*

A solution of the aldehyde **5** (6.67 g, 20 mmol), malonic acid (2.5 g, 24 mmol), piperidine (200 mg) in pyridine (20 cm^3) was heated under N_2 to 120 °C for 4 h. The solvent pyridine was removed, and the residual liquid upon silica gel chromatography using 95:5 $CHCl_3$/MeOH gave acid **6** (white solid, 6.83 g, 91%). Mp 113–114 °C (ether).

*2.3.4. p-(9-(2-Methylisoxazolidin-5-yl)nonyloxy)cinnamyl alcohol (**7**)*

To a solution of the acid **6** (5.00 g, 13.3 mmol) in ether (150 cm^3) at 0 °C was added $LiAlH_4$ (0.7 g, 18.4 mmol), and the mixture was stirred under N_2 at 0 °C for 1 h and 20 °C for another hour. The reaction mixture was quenched by successive addition of water (0.7 cm^3), 10% NaOH solution (0.7 cm^3) and water (2.8 cm^3). The white solid was washed with ether. The removal of ether afforded the alcohol **7** as a white solid (4.1 g, 85%). Mp 64–65 °C (ether).

*2.3.5. p-(9-(2-Methylisoxazolidin-5-yl)nonyloxy)cinnamaldehyde (**8**)*

A mixture of alcohol **7** (3.62 g, 10 mmol) in CH_2Cl_2 (150 cm^3) and MnO_2 (30 mmol) was stirred under N_2 at 20 °C for 96 h. After filtration and concentration, the residual product was purified over silica gel chromatography using an eluent of 99:1 Et_2O–MeOH mixture to give the aldehyde **8** as a white solid (2.7 g, 75%). Mp 60–61 °C (ether–pentane).

*2.3.6. Quaternization of adduct **8** with propargyl chloride: Synthesis of quaternary salt p-(9-[2-methyl-2-(2-popyn-1-yl) isoxazolidinium-5-yl]nonyloxy)cinnamaldehyde chloride **(10)***

A solution of the adduct **8** (2.0 g, 5.56 mmol) and propargyl chloride **9** (1.0 g, 13.4 mmol) in dry acetone (5 cm^3) was stirred under N_2 at 20 °C for 24 h. The salt started precipitating out within an hour. The removal of the solvent followed by washing the residue with ether (2×10 cm^3) gave a pale yellow solid of the chloride salt **10** (2.34 g, 97%).

2.4. Specimens

Corrosion study by gravimetric and electrochemical methods were carried out with mild steel coupons of the following composition: 0.089% (C), 0.037 (Cr), 0.34% (Mn), 0.022 (Ni), 0.010 (P), 0.007 (Mo), 0.005 (V), 0.005 (Cu), 99.47% (Fe). For the electrochemical tests, a 1 mm thick mild steel sheet was machined to a flag shape with an approximate stem of 3 cm. Insulating the stem by araldite (affixing material) provided 2 cm^2 exposed area which was abraded with increasing grades of emery papers (100, 400, 600 and 1500 grit size), washed with acetone deionized water. For the gravimetric test, the mild steel coupons were cleaned as

described above. The dried specimens were stored in a desiccator. Before their use, the electrode specimens were placed in an ultrasonic bath for 5 min, washed with distilled water and used immediately.

For autoclave tests, the two types of mild steel coupons have the following composition:

Coupon A: 0.082% (C), 0.016% (Cr), 0.207% (Mn), 0.062% (Ni), 0.029% (Cu), 0.012% (Mo), <0.001% (V), 0.032% (Si), <0.0005% (P), 0.0059% (S), 0.011% (Co), 0.045% (Al), <0.0010 (Nb), <0.0005% (Ti), <99.3% (Fe).
Coupon B: 0.168% (C), 0.038% (Cr), 0.495% (Mn), 0.034% (Ni), 0.074% (Cu), 0.0081% (Mo), 0.001% (V), 0.237% (Si), 0.014% (P), 0.024% (S), 0.011% (Co), 0.080% (Al), 0.0019 (Nb), 0.0015% (Ti), <98.6% (Fe).

2.5. Solutions

Reagent A.C.S. HCl and H_2SO_4 (Fisher Scientific Company) and distilled deionized water were used to prepare 1, 4 and 7.7 M HCl and 0.5 M H_2SO_4 solutions. Corrosion inhibition tests have been performed in 0.5 M NaCl in the presence of CO_2 (1 atm) at 40 °C as well as at higher pressure (10 bar) of CO_2 and temperature of 120 °C. Each solution was de-aerated with 99.999% N_2 (30 min) and then continuously saturated with 99.999% pure CO_2. The high purity CO_2 was used to avoid corrosion by oxygen. Studies using CO_2 gas showed that the corrosion at pH < 4 is mainly by reaction with H^+, while the active specie in less acidic solutions is adsorbed CO_2 or H_2CO_3 [28]. To avoid possible changes in the mechanism of the corrosion reaction, a solution of $NaHCO_3$ (100 mg/L) was used to maintain a pH between 5.0 and 5.5.

2.6. Gravimetric measurements

2.6.1. Gravimetric measurements in 0.5 M NaCl saturated with CO_2 (1 atm) at 40 °C, 1 M HCl, 4 M HCl, 7.7 M HCl and 0.5 M H_2SO_4 at 60 °C

For gravimetric measurements, the steel coupons measuring $2.5 \times 2.0 \times 0.1$ cm^3 were used. Inhibitor efficiency at 40 °C for 7 days was determined by hanging the steel coupon measuring $2.5 \times 2.0 \times 0.1$ cm^3 into a 0.5 M NaCl (150 cm^3) in the presence of CO_2 (1 atm) in the absence and presence of the inhibitors (200 ppm by weight). All subsequent concentrations of inhibitors were expressed in ppm by weight unless otherwise stated. At the end, the coupons were cleaned with distilled water, abraded lightly with emery paper, followed by washing with distilled water, acetone and drying at 110 °C.

The inhibition study in 1 M HCl and 0.5 M H_2SO_4 was carried out as above using acid solutions of 250 cm^3 for an immersion time of 6 h. For study using 4 and 7.7 M HCl, a solution volume of 500 cm^3 was used.

2.6.2. Gravimetric measurements at high temperature and pressure: Autoclave Experiments

The R&D Autoclave Bolted Closure System (Model # 401C-0679) used was procured from Autoclave Engineers. Its body and cover are made of SS316 and has two options of gaskets, namely, Teflon and SS316. This autoclave is designed to test the inhibitors at pressures up to 6000 psig (413 bar) and temperatures in excess of 1200 °F (648 °C). A glass liner was used to contain the corrosive liquid. Experiments were carried out using autoclave with a capacity of 1000 cm^3. The autoclave is equipped with temperature probe, pressure transducer, a spurger and a cooling coil. The autoclave is heated by an electrically heated jacket. A temperature probe inside the jacket measured the skin temperature of the autoclave. A feedback PID controller controlled the temperature inside the reactor. The temperature control and pressure read-out was done via a SCADA-HMI system specially designed for this application. The set-up through this system was attached to a microcomputer. In order to have a better control on the inside temperature, cooling water was used to reduce the temperature of the test solution.

Experiments were conducted at 10 bar and 120 °C in 0.5 M NaCl solution saturated with carbon dioxide to approximately simulate the conditions present in oil and gas field applications. The solution (250 cm^3) in the presence and absence of inhibitor molecules (200 ppm by weight) was poured into a temperature resistant glass liner, which was kept in the autoclave. Carbon dioxide was bubbled for 20 min to ensure that all dissolved oxygen was knocked off the test solution. Subsequently, the carbon-steel coupons prepared as described (*vide supra*) were immersed into the solution. The autoclave was closed using a torque wrench. After assembling the temperature and pressure sensors, the autoclave was pressurized to a desired level using carbon dioxide gas. A desired temperature was then set thru SCADA software. The system monitored the temperature and pressure through entire duration of the experiment for 48 h. The temperature history during a typical experiment showed its control within ±2 °C range.

2.7. Electrochemical measurements

2.7.1. Tafel extrapolation method

The polarization studies were carried out in a 250 cm^3 of 0.5 M NaCl solution in the presence of CO_2 (1 atm) in the absence and presence of various concentrations of inhibitors at 40 °C. The experiments were started only after a stable open circuit potential (OCP) was achieved usually within the exposure time of 30 min. The electrochemical cell, assembled in a 750 cm^3 round-bottomed flask, consisted of a saturated calomel electrode (SCE) as a reference electrode, mild steel working electrode, and the graphite counter electrode (≈5 mm diameter). The Bubbler has one outlet and inlet for the CO_2. The SCE electrode was connected to the cell using a Luggin–Haber capillary salt bridge, the tip of which was separated from the surface of the working electrode by a distance of ≈2 mm. An electrometer was used to connect all three electrodes to a Potentiostat (Model 283, EG&G PARC). A rate of 1.6 mV/s was used to scan a range of ±250 mV with respect to open circuit potential.

2.7.2. Linear polarization resistance (LPR) method

The cell described above was also used for the LPR measurement. The current potential plots (in a range of ±10 mV around E_{corr}) provided the polarization resistance values.

2.8. X-ray photoelectron spectroscopy

The metal coupons as treated in gravimetric tests in 1 M HCl at 60 °C for 6 h were gently rinsed with distilled deionized water and dried by gentle blowing of N_2. The coupons were kept inside a desiccator for XPS measurements. The XPS analysis was performed using a Thermos Scientific X-ray photoelectron spectrometer (Model # Escalab 250 Xi) and the samples were irradiated with monochromated Al K_α X-rays (1486.6 eV) of spot size of diameter 650 μm. The electron energy analyzer was operated in constant pass energy of 20 eV. The electron take of angle was 90°. Base pressure during analysis was in the 10^{-10} mbar range during the experiments. The spectra were referenced with C 1s peak at 285.1 eV. XPS spectra were deconvoluted using a non-linear least squares algorithm with a Shirley base line and a Gaussian–Lorentzian combination. Avantage software was used for all data processing.

3. Results

3.1. Synthesis of the corrosion inhibitors

The synthesis of the inhibitor molecules was achieved using nitrone-alkene cycloaddition protocol [43,44], which is indeed the best chemical template for the preparation of the isoxazolidines (Fig. 2). The nitrone-cycloaddition reactions are often used as a key step in the synthesis of many biologically important natural products [45]. The specialty alkene **3** bearing an aromatic aldehyde motif at the terminal of a hydrophobic alkyloxy chain was prepared *via* alkylation of *p*-hydroxybenzaldehyde **1** with 11-bromo-1-undecene **(2)**. The cycloaddition of nitrone **4** with **3** then gave isoxazolidine **5** in a very good yield. The Knoevenagel condensation of **5** with malonic acid gave **6** in excellent yield. The acid **6** upon $LiAlH_4$ reduction followed by MnO_2 oxidation afforded the much sought after substituted cinnamaldehyde **8**, which was then quaternized with propargyl chloride to give **10** in quantitative yield. Spectral data of the synthesized compounds are included in the Supplementary information. The rather arduous journey to synthesize the cinnamaldehydes is justified, since it has paved the way to evaluate the effect of multiple functionalities in a single molecule on the inhibition efficiencies. If promising, judicious choice of reactants would lead to other cinnamaldehydes using much simpler routes. It is highly gratifying to note that it has been possible to embed the cinnamaldehyde skeleton (to minimize hydrogen embrittlement), quaternary nitrogen (to impart solubility), hydrophobic spacer $(CH_2)_9$ (for surface coverage), propargyl moiety (to produce polymeric film) as well as an electron-rich aromatic moiety (for π-electron donation) in a single molecule **10**. All these functionalities are expected to impart corrosion inhibition. Note that the nitrogen in the isoxazolidine moiety is less basic (pK_b: ≈10.4) (because of the adjacent electronegative oxygen) but more nucleophilic in compare to a tertiary amine R_3N (pK_b: ≈4.2), due to the former having three repulsive adjacent lone pairs in the: N–Ö: group [15]. This is expected to make the isoxazolidine moiety in **5** and **8** a potent motif for chemisorption by nucleophilic electron donation to the metal surface. It has also been an interesting ploy to assemble a rather water-insoluble cinnamaldehyde moiety with the isoxazolidine ring where the unquenched valency of nitrogen can be manipulated to protonated $R^1R^2NH^+$ or $R^1R^2N^+CO_2^-$ (in the presence of CO_2) (as in the cases of **5**, **6** and **8**) or quaternary salt (**10**) so as to impart overall water-solubility. The ^1H NMR spectra of these interesting molecules **5**, **8** and **10** are shown in Fig. 3. Spectral analyses supported the assigned structure of the cycloaddition products. Note that each molecule of **5** or **8** is a mixture of two conformationally mobile invertomers of *cis*- and *trans*-disposed substituents at 2,5 positions; and the spectrum of **10** reveals the presence of two isomeric salts of *E* and *Z* disposition of the 2,5-substituents. To the best of our knowledge, it is the first time a cinnamaldehyde moiety is incorporated in a nitrone cycloaddition product (**8** or **10**).

Two commercial inhibitor samples **QI80-E**, an ethylsulfate of quaternized imidazolines (mixture having $R = C_{12}$ to C_{22}), from Materials Performance and **ARMOHIB 219** from AKZO NOBEL are also tested for the purpose of comparison (Fig. 2).

3.2. Gravimetric measurements

3.2.1. Measurements in 1 M HCl and 0.5 M H_2SO_4

The results of weight loss measurements at 60 °C after 6 h of immersion of coupons (in 1, 4, 7.7 M HCl and 0.5 M H_2SO_4) for the compounds **5**, **6**, **8**, and **10** are reported in Tables 1 and 2. Percent inhibition efficiency (η%) was calculated using Eq. (17):

$$\eta\% = \frac{\text{Weight loss (blank)} - \text{Weight loss (inhibitor)}}{\text{Weight loss (blank)}} \times 100 \qquad (17)$$

Triplicate determinations were made for each experiment. Where the masses of the coupons differed, relative weight loss of the coupons were used to calculate the η% using Eq. (18):

$$\eta\% = \frac{\Delta\overline{W}_o - \Delta W}{\Delta\overline{W}_o} \times 100 \qquad (18)$$

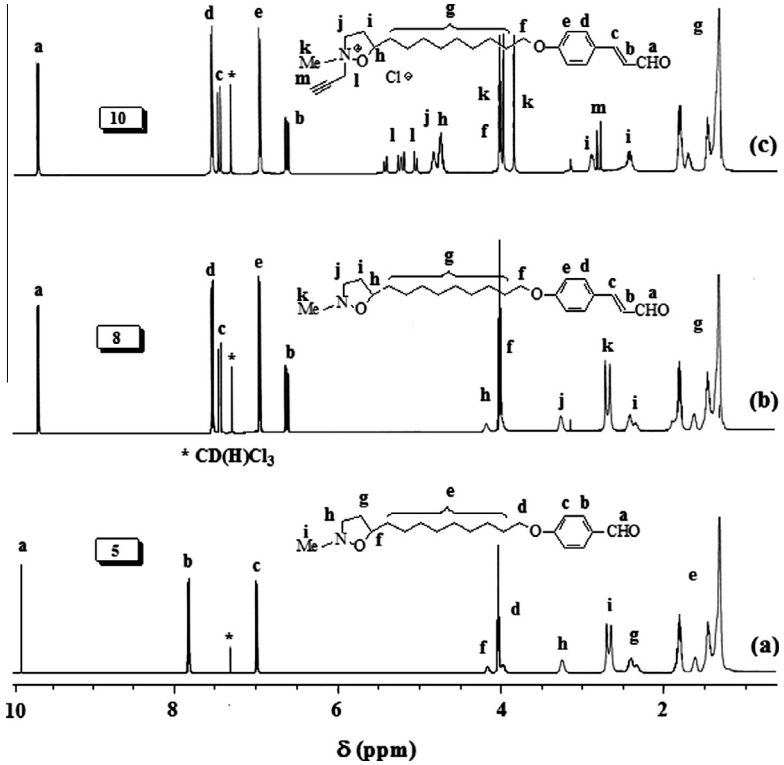

Fig. 3. ^1H NMR spectrum of (a) **5**, (b) **8**, and (c) **10** in $CDCl_3$.

Table 1
The η%[a,b] for different inhibitors for the inhibition of corrosion of mild steel exposed at 60 °C in 1 M HCl (6 h), 4 M HCl (3.75 h) and 7.7 M HCl (1.58 h).

Compound	η% at concentration of compounds (in ppm by weight) and HCl								
	5	10	25	50	100	200	400	50	50
	1.0 M HCl[b]							4.0 M HCl[c]	7.7 M HCl[d]
5[e]	67.9[c]	94.6	96.6	98.5	98.1	99.3	99.3	98.3	93.3
6[f]	71.5	87.3	95.1	98.1	98.7	99.3	99.7	91.3	87.2
8	72.2	93.8	95.4	98.6	98.9	99.2	99.4	92.3	88.2
10[g]	73.5	95.3	97.1	98.1	99.1	99.6	99.5	98.7	94.3

[a] IE (i.e., η) = surface coverage θ.
[b] Corrosion rate for a set of three blank experiments were found to be 55.8 ± 1.5 mm y^{-1}. The blanks repeated in several other occasions gave a CR within 1–3%.
[c] Corrosion rate for a set of three blank experiments were found to be 259 ± 9 mm y^{-1}.
[d] Corrosion rate for a set of three blank experiments were found to be 1610 ± 45 mm y^{-1}.
[e] 3 ppm, η% 53.8; 1 ppm, η% 27.8; 0.5 ppm, η% 16.5.
[f] 3 ppm, η% 58.3; 1 ppm, η% 33.3; 0.5 ppm, η% 21.4.
[g] 3 ppm, η% 64.3; 1 ppm, η% 38.5; 0.5 ppm, η% 27.3.

Table 2
The η%[a] for different concentrations of inhibitors for the inhibition of corrosion of mild steel exposed at 60 °C in 0.5 M H_2SO_4 (6 h).

Compound	η% at concentration (ppm by weight) of compounds						
	5	10	25	50	100	200	400
5	19.7	31.8	44.7	59.7	76.1	87.3	93.6
8	26.6	43.0	57.9	71.2	85.3	92.8	95.2
10	38.1	62.1	70.2	83.2	88.9	94.5	96.7

[a] Corrosion rate for a set of three blank experiments were found to be 61.7 ± 1.0 mm y^{-1}. The blanks repeated in several other occasions gave a CR within 1–3%.

where $\Delta\overline{W}_o$ and ΔW are the respective mean relative weight loss of the specimens in the blank and inhibitor solution. In Eqs. (19) and (20), W_{ib} and W_{fb} are the respective initial and final masses of the specimens in blank solutions while W_{is} and W_{fs} represent the corresponding masses in the inhibitor solution.

$$\Delta\overline{W}_o = \left[\sum (W_{ib} - W_{fb})/W_{ib}\right]/3 \tag{19}$$

$$\Delta W = (W_{is} - W_{fs})/W_{is} \tag{20}$$

The average η% reported in Tables 1 and 2 is found to have a standard deviation of 0.3–3.5%.

In a constant temperature bath, usually a set of over 20 experiments including three blanks were carried out simultaneously. For the blanks, three coupons of initial masses 4.1376, 4.0121 and 3.9505 g with respective surface area of 11.42, 11.41 and 10.90 cm^2, lost a mass of 0.3482, 0.3302 and 0.3354 g, respectively after 6 h immersion in 1 M HCl at 60 °C. Using equation: mm y^{-1} = (87.6 W/(DAT)) where W is weight loss in mgs, D density in g cm^{-3} (=7.87 g cm^{-3} for iron), A is the area in cm^2 and T is time in hours, the corrosion rates in mm y^{-1} were calculated and found to be 55.8 ± 1.5 mm y^{-1}. The blanks repeated in several other occasions gave a CR within 1–3%.

3.2.2. Measurements in CO_2-saturated 0.5 M NaCl at 1 atm

The results of weight loss measurements at 40 °C after 7 days of immersion for the compounds in 0.5 M NaCl solution in the presence of CO_2 (1 atm) are reported in Table 3. Duplicate determinations were made with each of the solutions.

3.2.3. Measurements in CO_2-saturated 0.5 M NaCl at high temperature and pressure

The results of the experiments carried out at temperature of 120 °C and a pressure of 10 bar CO_2 in 0.5 M NaCl for 48 h are given in Table 4. Duplicate determinations were made in each case. The steel coupon was weighed after the exposure and weight loss was determined. This information was used to calculate the corrosion rate in mm y^{-1} as before (*vide supra*).

Table 3
Corrosion inhibition efficiency, η (%) using polarization resistance, Tafel plots and gravimetric method of mild steel samples in various solutions containing 200 ppm by weight of the inhibitors in 0.5 M NaCl/CO_2 (1 atm) at 40 °C.

	η (%)		
Compound	Polarization method	Tafel method	Gravimetric method
5	90.5	95.5	96
8	97.8	95.6	96
10	97.6	98.5	97.8

3.3. Electrochemical measurements

3.3.1. Tafel extrapolation

The results of the Tafel plot extrapolation for mild steel in 1 M HCl (blank) at 60 °C or 0.5 M NaCl (blank) solutions containing various concentrations of the inhibitors at 40 °C in the presence of CO_2 (1 atm) are summarized in Tables 5 and 6. Some representative Tafel plots for the inhibition in 1 M HCl and in CO_2-saturated 0.5 M NaCl are shown in Figs. 4 and 5, respectively. It is worthwhile to mention that many Tafel plots do not have sufficient linear region to permit accurate extrapolation and determination of corrosion current density and Tafel slopes. In order to circumvent the problem, the data for the Tafel plots were analyzed by 352 SoftCorrII software, which utilizes the curve fitting procedure of an advanced numerical fit to the Butler–Volmer equation. The procedure does not require a fully developed linear region of the curve [46,47]. There is always a potential source of error in the values of corrosion current densities, which, in most cases, were obtained by extrapolation of cathodic Tafel lines to the respective free corrosion potential.

3.3.2. LPR

The η% from LPR technique was calculated using Eq. (21):

$$\eta(\%) = \left(\frac{R'_p - R_p}{R'_p}\right) \times 100 \tag{21}$$

Table 4
Corrosion rates and inhibition efficiencies of various corrosion inhibitors (200 ppm by weight) at 120 °C and 10 bar pressure of CO_2 in 0.5 M NaCl solution.

Solution	Coupon[a]	CR[b] (mm y^{-1})	% Inhibition	Average% Inhibition
BLANK	**A**	2.19	–	–
	B	2.23	–	
5	**A**	0.471	78.5	79.2
	B	0.457	79.8	
8	**A**	0.250	88.6	88.3
	B	0.270	87.9	
10	**A**	0.350	84.0	84.9
	B	0.319	85.7	
Q I 80	**A**	0.429	80.4	81.0
	B	0.410	81.6	
ARMOHIB219	**A**	0.396	81.9	82.7
	B	0.368	83.5	

[a] Two mild steel coupons **A** and **B** having different carbon content and compositions.
[b] Corrosion rate.

where R_p and R'_p are the respective polarization resistances in solution without or with the inhibitors in 1 M HCl at 60 °C and CO_2-saturated 0.5 M NaCl at 40 °C (Tables 5 and 7).

3.4. Adsorption isotherms

Surface coverage (θ, i.e. fractional inhibition efficiency η) values for the compounds studied are reported in Tables 1–7. The η is directly related to the surface coverage θ of the electrode by an inhibitor molecule at its lower concentration range, i.e., $\eta\% = \theta\%$. However, a transition from a monolayer to a multilayer coverage at higher inhibitor concentrations does no longer keep the relationship linear. The θ values obtained by gravimetric method in 1 M HCl (Table 1), and in 0.5 M H_2SO_4 (Table 2) and by Tafel extrapolations in CO_2-saturated 0.5 M NaCl (Table 6) and C (the concentration in ppm i.e. mg/kg was translated into mol/L) were used to find the best among the more frequently used adsorption isotherms [48,49], namely:

$$\text{Temkin}: \quad K_{ads}C = e^{f\theta} \tag{22}$$

$$\text{Langmuir}: \quad \theta/(1-\theta) = K_{ads}C \tag{23}$$

$$\text{Frumkin}: \quad K_{ads}C = \theta/(1-\theta)e^{-2a\theta} \tag{24}$$

$$\text{Freundluich}: \quad \theta = K_{ads}C^n \tag{25}$$

where K_{ads} is the equilibrium constant of the adsorption process. The correlation coefficient revealed the best fit for the Langmuir isotherm for the inhibitors in 1 M HCl [Fig. 6(a)] as well as in 0.5 M H_2SO_4 [Fig. 6(b)] and Temkin isotherm in CO_2 saturated 0.5 M NaCl [Fig. 6(c)] (Table 8). All the inhibitors in 1 M HCl also demonstrated

Table 6
Results of Tafel plots of a mild steel sample in various solutions containing inhibitor **5** in 0.5 M NaCl saturated with CO_2 at 40 °C.

Sample	Conc. (ppm)	Tafel plots				
		E_{corr} vs. *SCE* (mV)	β_a (mV/dec)	β_C (mV/dec)	i_{corr} (μA/cm^2)	η[a] (%)
Blank[b]	0	−695	67.1	−580	147	–
5	1.5	−659	66.1	−510	67.5	54.1
	2.5	−650	65.5	−418	54.9	62.7
	5	−647	52.0	−385	49.2	66.6
	10	−645	43.5	−300	38.4	73.9
	25	−640	34.7	−227	22.4	84.8
	100	−606	36.8	−247	7.90	94.6
	200	−601	35.6	−233	6.50	95.5
8	0.5	−681	94.5	−643	82.4	44.0
	1	−649	77.8	−337	47.9	67.4
	1.5	−646	67.4	−277	33.5	77.2
	2.5	−641	60.6	−228	17.5	88.1
	5	−633	93.8	−265	16.3	88.9
	10	−630	88.8	−255	14.1	90.4
	25	−621	81.4	−238	10.2	93.1
	100[c]	−617	73.1	−213	8.25	94.4
	200[c]	−607	77.3	−207	6.50	95.6
10	0.5	−690	68.7	−670	100	32.0
	1	−686	61.4	−376	70.5	52.0
	1.5	−681	69.8	−344	45.6	69.0
	2.5	−646	117	−259	17.9	87.9
	5	−635	123	−360	14.9	89.9
	10	−634	97.9	−279	12.1	91.8
	15	−618	110	−243	10.4	92.9
	25	−610	93.9	−241	8.00	94.6
	50	−596	128	−289	6.65	95.5
	100	−590	130	−280	2.88	98.0
	200	−586	125	−275	2.25	98.5

[a] Inhibition Efficiency, IE (i.e., η) = surface coverage θ.
[b] The blank was a 0.5 M NaCl solution saturated with CO_2.
[c] Cloudy solution.

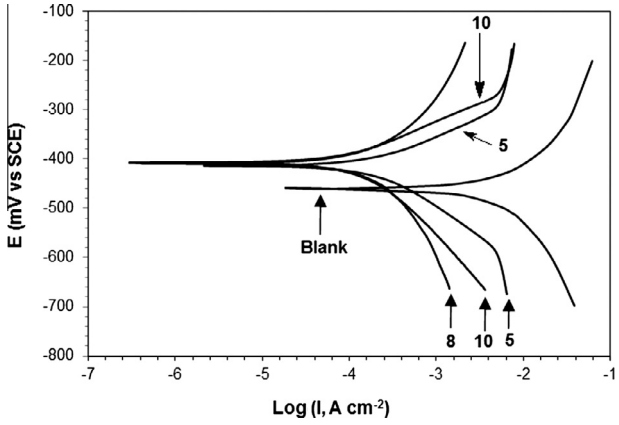

Fig. 4. Potentiodynamic polarization curves at 60 °C for mild steel in 1 M HCl containing 10 ppm of **5**, **8** and **10**.

Table 5
Results of Tafel plots in solutions containing 10 ppm by weight of the inhibitor in 1 M HCl at 60 °C.

Sample	Tafel plots					Polarization resistance	
	E_{corr} vs. *SCE* (mV)	β_a (mV/dec)	β_C (mV/dec)	i_{corr} (μA/cm^2)	%IE	R_p (Ω cm^2)	η (%)[b]
Blank[a]	−459	39.6	−94.5	786	–	24.3	–
5	−414	67.1	−98.5	114	85.5	180	86.5
8	−409	55.0	−81.9	57.6	92.7	248	90.2
10	−407	59.6	−103	65.6	91.7	250	90.3

[a] The blank was a 1 M HCl solution.
[b] Inhibition Efficiency, IE (i.e., η) = surface coverage θ.

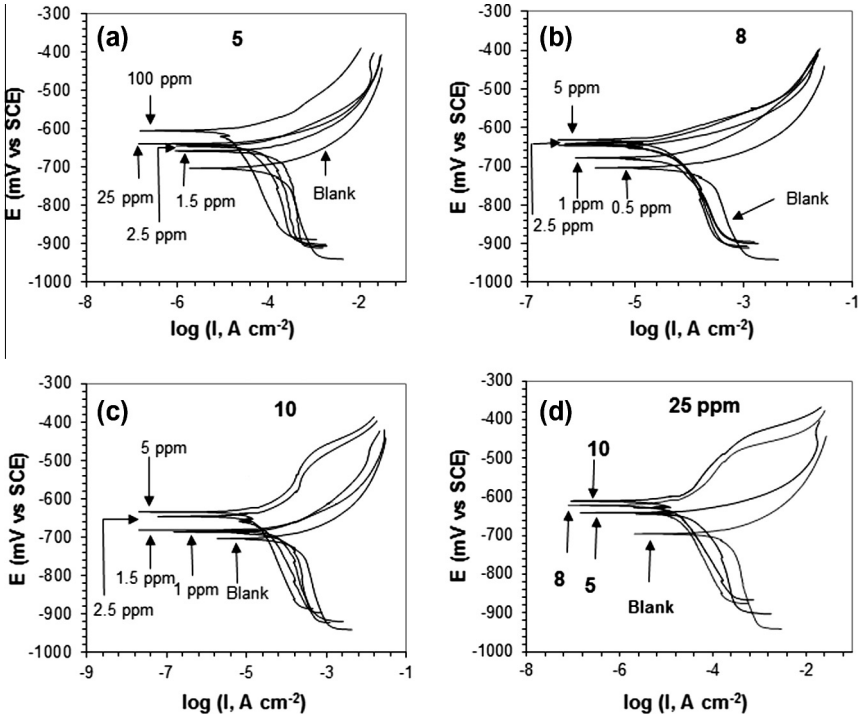

Fig. 5. Potentiodynamic polarization curves at 40 °C for mild steel in CO_2 Saturated 0.5 M NaCl containing different concentrations of (a) **5**, (b) imidazoline **8**, (c) **10** and (d) 25 ppm of **5**, **8** and **10**.

Table 7
Results of LPR method in 0.5 M NaCl saturated with CO_2 at 40 °C.

Sample	Concentration (ppm)	Polarization resistance		
		R'_p (Ω cm^2)	θ[a]	θ (%)
Blank[b]	0	129	–	–
5	1.5	343	0.623	62.3
	2.5	613	0.79	79.0
	5	689	0.813	81.3
	10	790	0.837	83.7
	25	980	0.868	86.8
	100	1057	0.878	87.8
	200	1360	0.905	90.5
8	1	351	0.632	63.2
	1.5	466	0.723	72.3
	2.5	763	0.831	83.1
	5	832	0.845	84.5
	10	1142	0.887	88.7
	25	1573	0.918	91.8
	100	3071	0.958	95.8
	200	5864	0.978	97.8
10	0.5	318	0.594	59.4
	1	357	0.639	63.9
	1.5	379	0.783	78.3
	2.5	1313	0.902	90.2
	5	1575	0.918	91.8
	10	1631	0.921	92.1
	15	2186	0.941	94.1
	25	3520	0.963	96.3
	50	5314	0.976	97.6
	100	5358	0.976	97.6
	200	5480	0.976	97.6

[a] Surface coverage, θ = Inhibition Efficiency, IE (i.e., η).
[b] 0.5 M NaCl saturated with CO_2.

good fit for the Temkin as well as Freundlich isotherms, while in 0.5 M H_2SO_4 inhibitors **5** and **8** also fitted well with the Temkin isotherm. The molecular interaction parameter f was calculated from linear fitting slope of $1/f$ [1] (Table 8) [49].

The K_{ads} is related to the free energy of adsorption (ΔG^{o}_{ads}), by:

$$K_{ads} = \frac{1}{55.5} \exp\left(\frac{-\Delta G^{o}_{ads}}{RT}\right) \quad (26)$$

The values of K_{ads} and ΔG^{o}_{ads} are summarized in Table 9.

3.5. X-ray photoelectron spectroscopy

The plots of the intensity (counts) vs. binding energy (eV) as measured by XPS are shown in Fig. 7. The results of the surface analysis are given in Table 10.

4. Discussion

The results of corrosion inhibition tests for the novel isoxazolidines containing a *p*-alkyloxycinnamaldehyde or *p*-alkyloxybenzaldehyde moiety in 1 M HCl as well as in 4 M and 7.7 M at 60 °C using weight loss method are included in Table 1. Compound **10** is an exciting molecule bearing cinnamaldehyde and alkyne moieties, both known for their inhibition abilities. All the inhibitor molecules **5**, **6**, **8** and **10** demonstrated very good η% as determined by gravimetric method. Inhibition efficiencies (η%) of ≈99% were achieved in the presence of 50 ppm of the inhibitor molecules. It is evident from Table 1 that the increase in the inhibitor concentration increases the η% to a limiting value which indicates the deposition of a monolayer film on the specimen. At an inhibitor concentration of 50 ppm, the effect of HCl strength on the inhibition efficiency (Table 1) revealed that the inhibitors performed very well in 4 M as well as in 7.7 M HCl. Inhibitor molecule **10** gave the best protection: at a concentration of 50 ppm, it gave η% of 98.1, 98.7 and 94.3 in 1 M, 4 M and 7.7 M HCl, respectively. The very good performance ascertains the efficacy of the functional motifs in the inhibitor molecules to arrest mild steel corrosion. Increasing HCl concentration was expected to decrease the inhibition efficiencies because of competition between H^+ and Inh^+ to

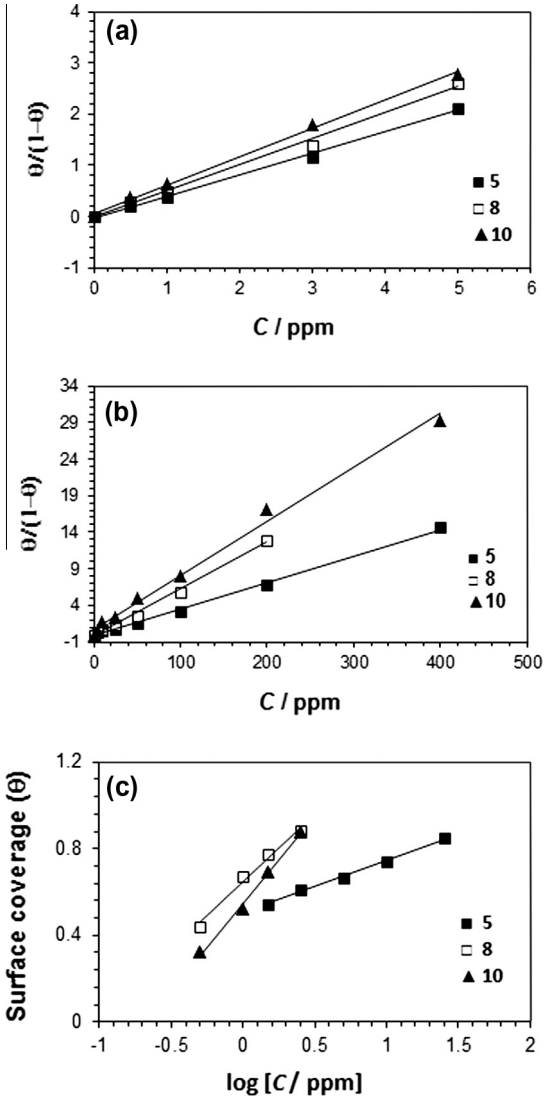

Fig. 6. (a) Langmuir adsorption isotherm of **5**, **8** and **10** in 1 M HCl at 60 °C, (b) Langmuir adsorption isotherm of **5**, **8** and **10** in 0.5 M H_2SO_4 at 60 °C and (c) Temkin adsorption isotherm of **5**, **8** and **10** in CO_2 Saturated 0.5 M NaCl at 40 °C.

Table 8
The square of correlation coefficients (R^2) and values of the constants (a, and f) in various adsorption isotherms in the presence of inhibitors.

Compound	Temkin (R^2, f)	Frumkin (R^2, a)	Langmuir (R^2)	Freundlich (R^2)
In 1 M HCl (60 °C) (Gravimetry)				
5	0.9923, 4.45	0.4096	0.9975	0.9936
8	0.9942, 4.52	0.1844	0.9958	0.9950
10	0.9953, 4.84	0.8319, −0.27	0.9972	0.9923
In 0.5 M H_2SO_4 (60 °C) (Gravimetry)				
5	0.9916, 5.65	0.4158	0.9972	0.9521
8	0.9935, 5.52	0.4148	0.9944	0.9097
10	0.9167, 7.87	0.5793	0.9934	0.8351
In 0.5 M NaCl/CO_2 (40 °C) (Tafel)				
5 (Tafel)	0.9942, 9.47	0.9499, −2.18	0.9568	0.9907
8 (Tafel)	0.9859, 3.64	0.9580, +0.680	0.9706	0.9544
10 (Tafel)	0.9936, 2.86	0.9010, +1.00	0.8861	0.9916
10 (LPR)	0.9955, 3.45	0.8741, +0.89	0.9324	0.9811

augment or arrest corrosion *via* reactions in Eqs. (6) and (9), respectively (*vide supra*). Nonetheless, increasing HCl concentration have a minimal effect on the η% (Table 1) thereby indicating

Table 9
Thermodynamic parameters of the mild steel dissolution in the presence of **5**, **8** and **10**.

Compound	Isotherm used	Slope[b]	K_{ads} (L/mol)[c]	ΔG^o_{ads} kJ/mol
In 0.5 M HCl (60 °C) (Gravimetry)				
5	Langmuir	0.4195	1.40×10^5	−43.9
8	Langmuir	0.5092	1.83×10^5	−44.6
10	Langmuir	0.5518	2.39×10^5	−45.4
In 0.5 M H_2SO_4 (60 °C) (Gravimetry)				
5	Langmuir	0.0362	1.21×10^4	−37.1
8	Langmuir	0.0637	2.29×10^4	−38.9
10	Langmuir	0.0736	3.20×10^4	−39.8
In 0.5 M NaCl/CO_2 (40 °C) (Tafel)				
5	Temkin	0.2431	3.89×10^7	−59.5
8	Temkin	0.6322	4.07×10^6	−53.1
10	Temkin	0.8056	2.07×10^6	−51.4
10[a]	Temkin	0.6675	4.02×10^6	−53.2

[a] *via* LPR.
[b] in Temkin Plot: slope = 2.303/f; in Langmuir Plot: slope = K_{ads}.
[c] K_{ads} obtained in L/mg was converted to L/mol.

the formation of a strongly adsorbed film on the metal surface as corroborated by XPS study (*vide infra*).

The results for the η% of the synthesized compounds (10 ppm) in 1 M HCl by Tafel extrapolations (Table 5) corroborated the findings of the weight loss method (Table 1). Significant lowering of the i_{corr} values confirms the inhibitive nature of the synthesized molecules. In the presence of the inhibitor molecules, the shifting of the E_{corr} in the positive direction 1 M HCl suggests that the synthesized molecules are anodic type inhibitors.

In the case of a shift of OCP by at least 85 mV in the presence of an inhibitor, it can be classified as a cathodic or anodic type inhibitor [50]. A displacement of 43–50 mV (Table 5) in the positive direction is not significant for the molecules to be considered as anodic type inhibitors. The more pronounced decrease in the anodic current densities is indicative of the greater decrease in the anodic oxidation rate than the rate of hydrogen evolution in the cathodic reaction. The inhibitors did not influence the corrosion reactions as indicated by the decreased values of slopes β_c and β_a; instead, they formed a barrier film on the metal surface. The above results suggest that the inhibitors are acting as mixed-type inhibitors under the major influence of anodic control. The very high η% may be attributed to the beneficial role of the π- and non-bonded electrons, hydrophobic alkyl chain, and the cinnamaldehyde group. These polarizable electrons assist the adsorption of the inhibitor molecules on the anodic sites through their interaction with the d-orbitals of iron or Fe^{2+}.

Next, we focused our attention to inhibition study in 0.5 M H_2SO_4 using weight loss method. To our satisfaction, the synthesized compounds showed very good inhibition efficacies (Table 2); η% in the range 94-97% in the presence of 400 ppm of inhibitor molecules were achieved. So far, the literature has documented only a few compounds, which are equally effective in arresting mild steel corrosion both in HCl and in H_2SO_4 media [8,51,52].

Finally, we focused on the main objective of the study: The investigation of corrosion inhibition in CO_2-saturated 0.5 M NaCl. The η% in the presence of 200 ppm of the inhibitor molecules as obtained from weight loss measurements at 40 °C after 7 days of immersion, Tafel extrapolation and linear polarization resistance are given in Table 3. To our great satisfaction, all three inhibitors showed very good inhibition efficiencies. The LPR and Tafel data corroborated the results obtained from the gravimetric method (Table 3). It is worth mentioning that gravimetry is the most simple yet the most reliable technique.

The results from the Tafel extrapolation and LPR in CO_2-saturated 0.5 M NaCl in the presence of various concentrations of the inhibitors are given in Tables 6 and 7, respectively. The

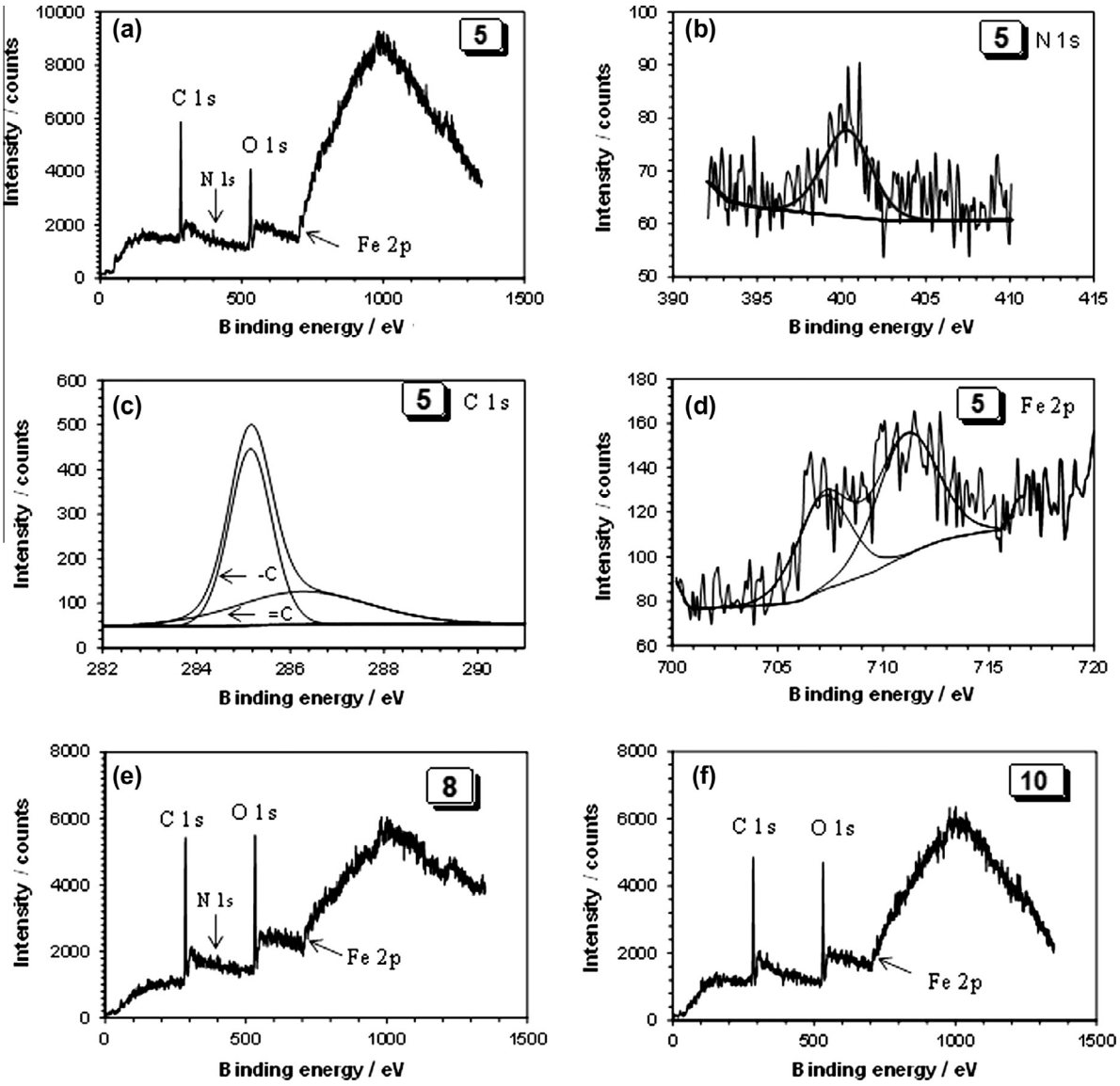

Fig. 7. (a) XPS spectrum of Fe after immersing into 1 M HCl at 60 °C for 6 h in the presence 100 ppm of inhibitor **5**; the XPS deconvoluted profiles of (b) N 1s, (c) C 1s, (d) Fe 2p; XPS spectra of Fe after immersing into 1 M HCl at 60 °C for 6 h in the presence 100 ppm of (e) inhibitor **8** and (f) **10**.

Table 10
XPS survey scan composition of Fe immersed in inhibited solution of 1 M HCl at 60 °C for 6 h.

Peak	Approx. binding energy (eV)	Composition (atom%)			C:N atom ratio	
		5	**8**	**10**	Calc.	Exp.
C 1s	285.1	42.8	45.5	51.4	**5** (20:1)	**5** (19.5:1)
C 1s	286.2	25.4	21.0	16.8	**8** (22:1)	**8** (24.6:1)
O 1s	530.1	6.8	5.0	4.5		
O 1s	532.6	18.9	24.4	25.5		
N 1s	400.3	3.5	2.7	0.0		
Fe 2p	711.0	1.5	1.4	1.2		
Fe 2p	707.0	1.1	0.0	0.6		

presence of inhibitors lowers the corrosion current density largely for the anodic branch than for the cathodic lines, thereby indicating the greater suppression of the anodic dissolution of the iron than the cathodic evolution of H_2 (Fig. 5). The inhibitor has shifted the E_{corr} in the positive direction in CO_2 saturated 0.5 M NaCl (Fig. 5 and Table 6). The E_{corr} values have shifted more than 85 mV in the positive direction in the higher concentration range for all three inhibitors. As a result, the compound can be classified as anodic type inhibitors [37]. This is supported by the observed increase in the anodic slopes (β_a) in the presence of the inhibitors, thereby confirming the influence of the inhibitors to suppress the anodic reactions.

For anodic polarization in the NaCl/CO_2 media containing inhibitors **8** (25 ppm) (Fig. 5d) and **10** (2.5, 5 and 25 ppm) (Fig. 5c and d), the curves have current-increasing plateau which are called the desorption potentials [53,54]. The desorption potentials at the concentrations of 2.5, 5 and 25 ppm of **10** were found to be −528, −500, −460 mV/SCE, respectively, while inhibitor **8** at a concentration of 25 ppm showed it at −474 mV/SCE. The desorption potential indicates that the mechanism of corrosion inhibition is influenced by the electrode potential. Note that Fig. 5c does not show any indication of desorption potential in the presence of lower concentrations (1 and 1.5 ppm) of **10**. The current-vs.-potential plots in Fig. 5a for various concentrations of **5** do not show any desorption potential. There seems to be a desorption potential for compound **8** at a concentration of 5 ppm while at 2.5 ppm the plot becomes normal (Fig. 5b). The results thus indicate that a

minimum critical concentration that can effectively cover the metal surface is required for the manifestation of the desorption potential. The degree of surface coverage (θ) depends on the bulk concentration of the inhibitors as well as on the electrode potential. Potentials higher than desorption potential lead to significant steel dissolution accompanied by desorption of the adsorbed inhibitors from the electrode surface. Observance of a desorption process of the inhibitor on the anodic polarization curves is suggestive of a mechanism by which the inhibitors block the anodic sites on the metal surface.

A negative or a positive value for the molecular interaction constant f indicates repulsion or attraction, respectively, among the adsorbed molecules [55]. The relatively lower positive values of f observed in 1 M HCl, 0.5 M H_2SO_4 as well as in CO_2-saturated 0.5 M NaCl indicate that there may be some van der Waal attractive forces among the hydrophobic nonamethylene chain (Table 6). The $-\Delta G^{o}_{ads}$ values for the adsorption process of inhibitor molecules **5**, **8** and **10** were calculated to be in the range 51–60 kJ/mol in 1 M HCl, 37–40 kJ/mol in 0.5 M H_2SO_4 and 44–45 kJ/mol in CO_2-saturated 0.5 M NaCl (Table 9). The relatively high negative values of ΔG^{o}_{ads} is suggestive of chemisorption of the inhibitor molecules on iron surface.

The presence of a variety of π and non-bonded electrons induces the synthesized compounds to interact with the anodic sites *via* overlapping with the low-lying vacant d-orbitals of iron. The presence of three lone pairs of electrons in the heteroatoms motifs: N–Ö: in the current isoxazolidines makes them more polarizable and powerful nucleophiles. The N—O motifs thus can undergo adsorption on the anodic sites through the interaction of its lone pairs with the d-orbitals of iron or deposited Fe^{2+} to provide a protective film [15].

Two types of metal coupons **A** and **B** having different elemental compositions and carbon content are used for the determination of η% in CO_2-saturated 0.5 M NaCl at higher temperature (120 °C) and pressure (10 bar, CO_2). To our great satisfaction, the synthesized inhibitors have imparted similar or even better (in the case of **8**) protection than the two commercial imidazolines **QI80** and **ARMOHIB219** (Table 4).

In XPS study, the presence of main element as carbon with small Fe content ascertains a carbonaceous surface indicative of the formation of a film covering the metal (Fig. 7, Table 10). The presence of N in small amounts was detected on the metal surface inhibited by **5** (Fig. 7a, b) and **8** (Fig. 7c), while it was not detected in the case of **10** (Fig. 7d). Note that the calculated C/N atom ratios of 20:1 and 22:1 in **5** and **8**, respectively, were found to be matched with the experimental findings of 19.5:1 and 24.6:1 (Table 10). The high carbon concentrations may only be related to the carbon rich structure of the inhibitors. We cannot offer a rationale for non-observance of N of inhibitor **10** on the metal surface. It is worth mentioning in this regard that the N in **10** is quaternary and in a sterically encumbered environment while the Ns in **5** and **8** are trivalent which can form coordinate bond on the metal surface.

The C 1s spectrum revealed a two-peak profile (Fig. 7c); the larger peak was assigned to the C—C aliphatic bonds with binding energy of 285.1 eV, whereas the peak at 286.2 was assigned to the C═C, C═O, and C—N bonds. The presence of O 1s peaks at 532.6 and 530.1 can be associated with molecule of the type N—O and O^{2-} thereby implying the interaction between the inhibitors and the oxide layer on the metal surface [56,57]. Small intensity peaks at 711 and 707 are indicative of the presence of Fe^{3+} (2p) and Fe^{0} (2p) (Fig. 7d).

5. Conclusions

A novel compound **10** having cationic charge, hydrophobic spacer of $(CH_2)_9$, electron-rich aromatic ring, alkyne and cinnamyl motifs has been synthesized using nitrone cycloaddition reaction as a key step. The compound **10** as well as its precursor molecules **5** and **8** are among a rare class of molecules, which are found to be very good corrosion inhibitors in HCl, H_2SO_4 and CO_2-saturated saline media. At a concentration of 25 ppm at 40 °C, inhibitor molecules **5**, **8** and **10** imparted an IE of 84.8, 93.1 and 94.6%, respectively in CO_2-saturated 0.5 M NaCl (Table 6). The IE of some of the synthesized molecules for test under high pressure of 10 bar and temperature of 120 °C were found to be similar or even better as compared to two commercial inhibitors tested for this purpose. In the presence of 200 ppm, the inhibitor molecules **5**, **8**, **10**, and commercial inhibitors QI 80 and ARMOHIB 219 demonstrated η% of 79.2, 88.3, 84.9, 81.0 and 82.7, respectively. The ΔG^{o}_{ads} point towards both physisorption as well as chemisorption of the inhibitors on the metal surface. The interesting findings from the current work would indeed be helpful in judicious designing, synthesis and corrosion inhibition study of isoxazolidines or other class of compounds containing an assembly of several structural features beneficial to inhibit corrosion The presence of electron-rich aromatic moiety at the end of the hydrophobic tail in the inhibitors may help to lock them strongly on the metallic surface. The compounds act mainly as anodic inhibitors. While the adsorption process in HCl and H_2SO_4 follows the Langmuir adsorption isotherm, it obeys Temkin adsorption isotherm in CO_2-satuarted/saline media.

Acknowledgements

Facilities provided by King Fahd University of Petroleum and Minerals and financial assistance by King Abdulaziz City of Science and Technology (KACST) (under the Grant: AR-26-26) and Deanship of Scientific Research, KFUPM (Startup Grant: IN121036) are gratefully acknowledged.

Appendix A. Supplementary material

Supplementary data associated with this article can be found, in the online version, at http://dx.doi.org/10.1016/j.corsci.2014.06.026.

References

[1] W. Durnie, B. Kinsella, R. De Marco, A. Jefferson, Structure activity of oil field corrosion inhibitors, J. Electrochem. Soc. 146 (1999) 1751–1756.
[2] S. Ghareba, S. Omanovic, Interaction of 12-aminododecanoic acid with a carbon steel surface: towards the development of 'green' corrosion inhibitors, Corros. Sci. 52 (2010) 2104–2113.
[3] F.M. Song, A comprehensive model for predicting CO_2 corrosion rate in oil and gas production and transportation systems, Electrochim. Acta 55 (2010) 689–700.
[4] X. Jiang, Y.G. Zheng, D.R. Qu, W. Ke, Effect of calcium ions on pitting corrosion and inhibition performance in CO_2 corrosion of N80 steel, Corros. Sci. 48 (2006) 3091–3108.
[5] K. Mallaiya, R. Subramaniam, S.S. Srikandan, S. Gowri, N. Rajasekaran, A. Selvaraj, Electrochemical characterization of the protective film formed by the unsymmetrical Schiff's base on the mild steel surface in acid media, Electrochim. Acta 56 (2011) 3857–3863.
[6] K. Aramaki, N. Hagiwara, H. Nishihara, The synergistic effect of anions and the ammonium cation on the inhibition of iron corrosion in acid solution, Corros. Sci. 27 (1987) 487–497.
[7] A. Khamis, M.M. Saleh, M.I. Awad, Synergistic inhibitor effect of cetylpyridinium chloride and other halides on the corrosion of mild steel in 0.5 M H_2SO_4, Corros. Sci. 66 (2013) 343–349.
[8] D. Daoud, T. Douadi, S. Issaadi, S. Chafaa, Adsorption and corrosion inhibition of new synthesized thiophene Schiff base on mild steel X52 in HCl and H_2SO_4 solutions, Corros. Sci. 79 (2014) 50–58.
[9] L.I. Antropov, The application of the potential scale to the problem of the corrosion and protection of metals, Zh. Fiz. Khim. 37 (1963) 965–978.
[10] S. Rengamani, S. Muralidharan, M.A. Kulandainathan, S.V. Iyer, Inhibiting and accelerating effects of amino phenols on the corrosion and permeation of hydrogen through mild-steel in acidic solutions, J. Appl. Electrochem. 24 (1994) 355–360.
[11] T. Basu, D. Nandi, P. Sen, U.C. Ghosh, Equilibrium modeling of As(III, V) sorption in the absence/presence of some groundwater occurring ions by iron(III)-cerium(IV) oxide nanoparticle agglomerates: a mechanistic approach of surface interaction, Chem. Eng. J. 228 (2013) 665–678.

[12] W.J. Lorenz, Theory of partial charge transfer reactions, Z. Phys. Chem. (Leipzig) 244 (1970) 65–84.
[13] A. Popova, E. Sokolova, S. Raicheva, M. Chirstov, AC and DC study of temperature effect on mild steel corrosion in acid media in presence of benzimidazole derivatives, Corros. Sci. 45 (2003) 33–58.
[14] S.A. Ali, M.T. Saeed, S.U. Rahman, The isoxazolidines: a new class of corrosion inhibitors of mild steel in acidic medium, Corros. Sci. 45 (2003) 253–266.
[15] S.A. Ali, A.M. El-Shareef, R.F. Al-Ghamdi, M.T. Saeed, The isoxazolidines: the effects of steric factor and hydrophobic chain length on the corrosion inhibition of mild steel in acidic medium, Corros. Sci. 47 (2005) 2659–2678.
[16] S.A. Ali, H.A. Al-Muallem, M.T. Saeed, S.U. Rahman, Hydrophobic-tailed bicycloisoxazolidines: a comparative study of the newly synthesized compounds on the inhibition of mild steel corrosion in hydrochloric and sulfuric acid media', Corros. Sci. 50 (2008) 664–675.
[17] S.A. Ali, H.A. Al-Muallem, S.U. Rahman, M.T. Saeed, Bis-isoxazolidines: a new class of corrosion inhibitors of mild steel in acidic media, Corros. Sci. 50 (2008) 3070–3078.
[18] S.A. Ali, A.J. Hamdan, A.A. Al-Taq, S.M.J. Zaidi, M.T. Saeed, In search of a functionality for an efficient inhibition of mild steel corrosion both in HCl and H_2SO_4, Corros. Eng. Sci. Technol. 46 (2011) 796–806.
[19] M.A. Hegazy, M. Abdallah, M.K. Awad, M. Rezk, Three novel di-quaternary ammonium salts as corrosion inhibitors for API X65 steel pipeline in acidic solution. Part I: Experimental results, Corros. Sci. 81 (2014) 54–64.
[20] D. Jayaperumal, S. Muralidharan, P. Subramanium, G. Venkatachari, S. Senthilvel, Propargyl alcohol as hydrochloric acid inhibitor for mild steel-temperature dependence of critical concentration, Anti-Corros. Methods Mater. 44 (1997) 265–268.
[21] Y.G. Avdeev, Y.I. Kuznetsov, A.K. Buryak, Inhibition of steel corrosion by unsaturated aldehydes in solutions of mineral acids, Corros. Sci. 69 (2013) 50–60.
[22] M. Gopiraman, N. Selvakumaran, D. Kesavan, I.S. Kim, R. Karvembu, Chemical and physical interactions of 1-Benzoyl-3,3-disubstituted thiourea derivatives on mild steel surface: Corrosion inhibition in acidic media, Ind. Eng. Chem. Res. 51 (2012) 7910–7922.
[23] X. He, Y. Jiang, C. Li, W. Wang, B. Hou, L. Wu, Inhibition properties and adsorption behavior of imidazole and 2-phenyl-2-imidazoline on AA5052 in 1.0 M HCl solution, Corros. Sci. 83 (2014) 124–136.
[24] G. Zhang, C. Chen, M. Lu, C. Chai, Y. Wu, Evaluation of inhibition efficiency of an imidazoline derivative in CO_2-containing aqueous solution, Mater. Chem. Phys. 105 (2007) 331–340.
[25] U. Lotz, L. Van Bodegom, C. Ouwehand, The effect of type of oil or gas condensate on carbonic acid corrosion, Corrosion 47 (1991) 635–644.
[26] K. Chokshi, W. Sun, S. Nesic, Iron carbonate scale growth and the effect of inhibition in CO2 corrosion of mild steel, NACE International Corrosion Conference & Expo, Paper No. 05285, 2005.
[27] F. Farelas, M. Galicia, B. Brown, N. Nesic, H. Castaneda, Evolution of dissolution processes at the interface of carbon steel corroding in a CO_2 environment studied by EIS, Corros. Sci. 52 (2010) 509–517.
[28] K. Videm, A. Dugstad, Corrosion of carbon–steel in an aqueous carbon-dioxide environment. Part 1: solution effects, Mater. Performance 28 (1989) 63–67.
[29] Y.J. Tan, S. Bailey, B.B. Kinsella, An investigation of the formation and destruction of corrosion inhibitor films using electrochemical impedance spectroscopy (EIS), Corros. Sci. 38 (1996) 1545–1561.
[30] V. Jovancicevic, S. Ramachandran, P. Prince, Inhibition of carbon dioxide corrosion of mild steel by imidazolines and their precursors, Corrosion 55 (1999) 449–455.
[31] F. Bentiss, M. Triasnel, H. Vezin, M. Lagrenee, Linear resistance model of the inhibition mechanism of steel in HCl by triazole and oxadiazole derivatives: structure-activity correlations, Corros. Sci. 45 (2003) 371–380.
[32] S.L. Wu, Z.D. Cui, F. He, Z.Q. Bai, S.L. Zhu, X.J. Yang, Characterization of the surface film formed from carbon dioxide corrosion on N80 steel, Mater. Lett. 58 (2004) 1076–1081.
[33] T. Berntsen, M. Seiersten, T. Hemmingsen, Effect of $FeCO_3$ supersaturation and carbide exposure on the CO_2 corrosion rate of carbon steel, Corrosion 69 (2013) 601–613.
[34] S. Nesic, K.L.J. Lee, A mechanistic model for carbon dioxide corrosion of mild steel in the presence of protective iron carbonate films-part 3: film growth model, Corrosion 59 (2003) 616–627.
[35] X. Liu, S. Chen, H. Ma, G. Liu, L. Shen, Protection of iron corrosion by stearic acid and stearic imidazoline self-assembled monolayers, Appl. Surf. Sci. 253 (2006) 814–820.
[36] X. Liu, P.C. Okafor, Y.G. Zheng, The inhibition of CO_2 corrosion of N80 mild steel in single liquid phase and liquid/particle two-phase flow by amino ethyl imidazoline derivatives, Corros. Sci. 51 (2009) 744–751.
[37] P.C. Okafor, X. Liu, Y.G. Zheng, Corrosion inhibition of mild steel by ethylamino imidazoline derivative in CO_2-saturated solution, Corros. Sci. 51 (2009) 761–768.
[38] F. Farelas, A. Ramirez, Carbon dioxide corrosion inhibition of carbon steels through bis-imidazoline and imidazoline compounds studied by EIS, Int. J. Electrochem. Sci. 5 (2010) 797–814.
[39] X. Liu, Y.G. Zheng, Effect of hydrophilic group on inhibition behaviour of imidazoline for CO_2 corrosion of N80 in 3% NaCl solution, Corros. Eng. Sci. Technol. 43 (2008) 87–92.
[40] M.W.S. Jawich, G.A. Oweimreen, S.A. Ali, Heptadecyl-tailed mono- and bis imidazolines: a study of the newly synthesized compounds on the inhibition of mild steel corrosion in a carbon dioxide-saturated saline medium, Corros. Sci. 65 (2012) 104–112.
[41] A. Edwards, C. Osborne, S. Webster, D. Klenerman, M. Joseph, P. Ostovar, M. Doyle, Mechanistic studies of the corrosion inhibitor oleic imidazoline, Corros. Sci. 36 (1994) 315–325.
[42] G. McIntire, J. Lippert, J. Yudelson, The effect of dissolved CO2 and O2 on the corrosion of iron, Corrosion 46 (1990) 91–95.
[43] J.J. Tufariello, in: A. Padwa (Ed.), 1,3-Dipolar Cycloaddition Chemistry, Wiley-Interscience, New York, 1984.
[44] P.N. Confalone, E.E. Huie, The (3 + 2) nitrone-olefin cycloaddition reaction, Organ. React. 36 (1988) 1–173.
[45] H. Ida, C. Kibyasi, Natural product using nitrones cycloaddition reaction, Yuki Gosei Kagaku Kyokaishi 41 (1983) 652–666.
[46] A. Fossati, F. Borgioli, E. Galvanetto, T. Bacci, Corrosion resistance properties of plasma nitrided Ti–6Al–4V alloy in nitric acid solutions, Corros. Sci. 46 (2004) 917–927.
[47] Z. Cai, T. Shafer, I. Watanabe, M.E. Nunn, Toru Okabe, Electrochemical characterization of cast titanium alloys, Biomaterials 24 (2003) 213–218.
[48] A.N. Frumkin, Die Kapillarkurve der höheren Fettsäuren und die Zustandsgleichung der Oberflächenschicht, Z. Phys. Chem. 116 (1925) 466–484.
[49] J.O'M. Bockris, S.U.M. Khan, Surface Electrochemistry: A Molecular Level approach, Plenum press, New York and London, 1993.
[50] O.L. Riggs Jr., Corrosion Inhibitors, second ed., C. C. Nathan, Houston, TX, 1973.
[51] X. Li, S. Deng, H. Fu, Inhibition of the corrosion of steel in HCl, H_2SO_4 solutions by bamboo leaf extract, Corros. Sci. 62 (2012) 163–175.
[52] X. Li, S. Deng, H. Fu, Triazolyl blue tetrazolium bromide as a novel corrosion inhibitor for steel in HCl and H_2SO_4 solutions, Corros. Sci. 53 (2011) 302–309.
[53] F. Bentiss, M. Traisnel, M. Lagreneea, The substituted 1, 3, 4-oxadiazoles: a new class of corrosion inhibitors of mild steel in acidic media, Corros. Sci. 42 (2000) 127–146.
[54] W. Jia, A study on the impedance responses of inhibitor desorption, Chin. J. Oceanol. Limnol. 16 (1998) 54–59.
[55] A. Yurt, G. Bereket, A. Kivrak, A. Balaban, B. Erk, Effect of Schiff bases containing pyridyl group as corrosion inhibitors for low carbon steel in 0.1 M HCl, J. Appl. Electrochem. 35 (2005) 1025–1032.
[56] O. Olivares-Xometl, N.V. Likhanova, M.A. Domínguez-Aguilar, J.M. Hallen, L.S. Zamudio, E. Arce, Surface analysis of inhibitor films formed by imidazolines and amides on mild steel in an acidic environment, Appl. Surf. Sci. 252 (2006) 2139–2152.
[57] M. Tourabi, K. Nohair, M. Traisnel, C. Jama, F. Bentiss, Electrochemical and XPS studies of the corrosion inhibition of carbon steel in hydrochloric acid pickling solutions by 3,5-bis(2-thienylmethyl)-4-amino-1,2,4-triazole, Corros. Sci. 75 (2013) 123–133.